

QUASI-PERIODIC VIBRATION EXCITATION MECHANISMS DUE TO TWO-PHASE CROSS FLOW IN STEAM GENERATOR TUBE BUNDLES

Changqing Zhang, Michel Pettigrew, Njuki Mureithi,
École Polytechnique

1. INTRODUCTION

Two-phase cross flow exists in many shell-and-tube heat exchangers, for instance, in the U-tube region of nuclear steam generators. Flow-induced vibration excitation forces can cause tube motion that will result in long-term fretting-wear or fatigue. To prevent these tube failures in heat exchangers, designers and troubleshooters must have guidelines that incorporate flow-induced vibration excitation forces.

In single-phase flow, these forces have been extensively measured and analyzed. They have been related to periodic wake shedding and to the turbulence level created by the tube bundle itself. Experimental data obtained for different kinds of fluids and tube bundles have been satisfactorily compared through the use of adequate data-reduction procedures [1, 2].

In the case of two-phase flows, such an extensive study has not been undertaken, though it is known that there are significant differences between single- and two-phase situations. In particular, the relationship between the two phases must be considered in addition to another parameter that is void fraction. This results in different flow regime or patterns of two-phase flow. A few sets of experimental results have been obtained recently, as in Refs [2-12]. However many questions remain such as the effects of viscosity, surface tension, density ratio or flow regimes. Actually, the main problem is the understanding of the physical mechanism that induces these forces. Detailed flow and vibration excitation force measurements in tube bundles subjected to two-phase cross flow are required to understand the underlying vibration excitation mechanisms. Some of this work has already been done by Pettigrew et al. [11] and Zhang et al. [12]. The distributions of both void fraction and bubble velocity in rotated-triangular tube bundles were obtained. Somewhat unexpected but significant quasi-periodic forces in both the drag and lift directions were measured.

The present work aims at understanding the nature of such unexpected drag and lift quasi-periodic forces. An experimental program was carried out with two rotated-triangular tube arrays of different width subjected to air/water flow to simulate two-phase mixtures. Fiber-optic probes were developed to measure local void fraction. Both the dynamic lift and drag forces were measured with strain gage instrumented cylinders.

The investigation showed that the quasi-periodic drag and lift forces are generated by different mechanisms that have not been observed so far. The quasi-periodic drag forces appear related to the momentum flux fluctuations in the main flow path between the cylinders. These kinds of momentum flux fluctuations are caused by void fraction fluctuations in the main flow path between the cylinders. The quasi-periodic lift forces, on the other hand, are mostly correlated to oscillations in the wake of the cylinders. The quasi-periodic lift forces are related to local void fraction measurements in the unsteady wake area between upstream and downstream cylinders. The quasi-periodic drag forces correlate well with similar measurements in the main flow stream between cylinders.

2. EXPERIMENTAL CONSIDERATIONS

2.1 Test Sections

The experiments were done in an air-water loop to simulate two-phase flows. The loop was described in details by Pettigrew et al. [11] or Zhang et al. [12]. Compressed air was injected below a suitably designed mixer to homogenize and distribute the two-phase mixture uniformly below the test-section. The air flow was measured with orifice plates connected to a differential pressure transducer and electronic readout system. The loop was operated at room temperature and the pressure in the test section was slightly above atmospheric.

The narrow test section, which has an essentially rectangular cross section (99×191mm), is shown in Figs 1(a) and 1(b). It consists of a column of six 38 mm diameter cylinders flanked on either side by half cylinders to simulate essentially the flow path in a large array of cylinders in a rotated triangular configuration. The pitch-to-diameter ratio, P/D , was 1.5 resulting in an inter-cylinder gap of 19 mm which allowed sufficient space for detailed flow measurements. The test-section length-to-gap width ratio is ten, thus, adequate to maintain essentially two-dimensional flow. The measurements were taken at several positions with fiber-optic probes assembled within a traversing mechanism. The tip of the probes could be positioned accurately with a micrometer head. The wider test section is similar but includes three columns of cylinders instead of one (Fig. 1(c)). It was used to verify the existence of periodic drag and lift forces in a more realistic configuration.

The probe assemblies were installed at four principal positions in the array as shown in Fig. 1(a). These positions are henceforth called lower and upper 60° (L60° and U60°) for the narrow gaps between cylinders and lower and upper 90° (L90° and U90°) for the larger flow areas between upstream and downstream cylinders. One cylinder was instrumented with strain gauges to measure the dynamic drag and lift forces due to the two-phase flow.

2.2 Fiber-optic probes for two-phase flow measurements

Each fiber-optic probe has a conical tip and is made of an optical fiber of 170 μm diameter. It acts as a phase sensor based on the different level of light reflection between air and water (Fig. 2). Four probes were used to measure simultaneously the dynamic characteristics of two-phase flow surrounding the instrumented cylinder. Several different probe combinations as shown in Fig. 3 were selected for two-phase flow measurements, i.e., LLLL, CCCC, RRRR, etc. Here L, C and R represent the left, center and right positions of probe L60°, L90°, U60° and U90° in the main flow path, respectively. Additionally L_0 is a point on the center line of the test section at the Probe U90° position. L_1 is about 5 mm from L_0 .

2.3 Instrumentation

Both the dynamic lift and drag forces were measured with a strain gage instrumented cylinder located in the fifth position (C5-N) from the upstream end of the narrow test-section (Fig. 1(a)). The instrumented cylinder was cantilevered and surrounded by rigid tubes. Two pairs of diametrically opposite strain gages were installed in the cylinder at 90 deg from each other to measure the forces in the flow direction (drag) and in the direction normal to the flow (lift). The strain gages were connected to strain indicators. The natural frequency of the cantilever cylinders was much higher (i.e., >150Hz) than the excitation force frequencies such that the cantilever

cylinder functioned essentially as a dynamic force transducer. The static strain-force relation was determined via a careful calibration.

Two-phase flow and the dynamic lift and drag force measurements in the narrow test section were performed simultaneously. Four flow conditions were investigated in detail, i.e., 80% and 90% volumetric void fractions at a nominal pitch flow velocity, U_p , of 5 m/s and 10 m/s. Both the void probe and the force signals were analyzed on an OR38 8-32 channel real time multi-analyzer/recorder coupled to a laptop computer.

3. EXPERIMENTAL RESULTS AND DISCUSSION

3.1 Dynamic lift and drag force measurements

Detailed vibration excitation force measurements in a rotated triangular tube bundle subjected to two-phase cross flow have been taken by Zhang et al. [12]. The experiments revealed somewhat unexpected but significant quasi-periodic forces in both the drag and lift directions. These forces are significantly larger in the drag direction. However, the excitation force frequency is relatively low (i.e., 3-6 Hz) and not directly dependent on flow velocity in the drag direction. On the other hand much higher frequencies (up to 16 Hz) were observed in the lift direction for 80% void fraction at 10 m/s pitch flow velocity. The frequency appears directly related to flow velocity in the lift direction. The periodic forces appeared well correlated along the cylinder with the drag force somewhat better correlated than the lift forces. The periodic forces are also dependent on the position of the cylinder within the bundle.

For the purpose of understanding the nature of these unexpected drag and lift quasi-periodic forces, force measurements were taken with an instrumented cylinder located in the fifth cylinder position (C5-N) from the upstream end of the narrow test-section (Fig. 1(a)). Typical lift and drag force spectra are shown in Fig. 4. The spectra reveal narrow band or quasi-periodic forces. For the case of 80% void fraction, the periodic force frequency in the lift direction increases from about 11 to 16 Hz for a corresponding increase in pitch flow velocity of 5 to 10 m/s (Figs 4(a) and 4(c)). This yields Strouhal numbers (fD/U_p) from 0.08 to 0.06. Although periodic wake shedding was not believed to have occurred at such high void fraction, the wake between cylinders was observed visually to be quite unsteady.

Periodicity was also observed in the drag direction as shown in Figs 4(b) and 4(d). Surprisingly, for the case of 80% void fraction, the frequency of the periodic drag forces is relatively low and does not change so much (4 Hz for 5 m/s, 4.625 Hz for 10 m/s), and these forces are significantly larger. Some very sharp peaks at low frequency (around 2 Hz) also appeared at high mass fluxes as shown in Fig. 4(d). They were found to be unwanted pump noise and not considered further.

3.2 Dynamic characteristics of two-phase flow

The detailed flow measurements previously taken by Pettigrew et al. [11] show that the flow tends to stream between the cylinders and that within that stream the flow velocity is fairly uniform but the void fraction distribution is not. In fact, the flow path resembles a series of two-dimensional 60° elbows as shown in Fig. 3.

In this paper only the dynamic characteristics of the two-phase flow in terms of local void fraction fluctuations are considered. The original void fraction fluctuation signals were processed into 0-1 ideal signals, where 0 means liquid phase and 1 means gas phase. The power spectra of the local void fraction fluctuation detected by the fiber-optic probes were analyzed. Typical

power spectra of the local void fraction fluctuation on the right side of the main flow path are shown in Fig. 5. The power spectra show the non-random and somewhat narrow band characters of the void fraction fluctuation. For the case of 80% void fraction, at 5 m/s pitch flow velocity (Figs 5(a), (b), (c) and (d)), the spectra have a dominant frequency of about 4 Hz; at 10 m/s pitch flow velocity (Figs 5(e), (f), (g) and (h)), the spectra have a dominant frequency of about 4.6 Hz. These dominant frequencies are consistent with those of the dynamic drag forces (Figs 4(b) and 4(d)). This clearly indicates a possible dynamic link between the void fraction fluctuation on the right side of the main flow path and the dynamic drag forces.

Typical power spectra of the local void fraction fluctuation on the left side of the main flow path are shown in Fig. 6. They also show the non-random and somewhat narrow band character of the void fraction fluctuation. For 80% void fraction, at 5 m/s pitch flow velocity (Figs 6(a), (b), (c) and (d)), the spectra have a dominant frequency of about 11 Hz; at 10 m/s pitch flow velocity (Figs 6(e), (f), (g) and (h)), the spectra have a dominant frequency of about 16 Hz. These dominant frequencies are consistent with those of the dynamic lift forces (Figs 4(a) and 4(c)). This clearly indicates a possible dynamic link between the void fraction fluctuation on the left side of the main flow path and the dynamic lift forces. Furthermore, the void fraction fluctuations at that location are probably caused by the flow oscillation in the wake between the upstream and downstream cylinders. These flow oscillations were observed visually during the tests. Some less prominent low frequency peaks are also shown in Fig. 6: at 5 m/s pitch flow velocity (Figs 6(a), (b), (c) and (d)), a low frequency peak is at about 4 Hz; at 10 m/s pitch flow velocity (Figs 6(e) and 6(g)), a low frequency peak exists around 4.6 Hz. These frequencies are also present in the dynamic drag force spectra (Figs 4(b) and 4(d)).

Typical power spectra of the local void fraction fluctuation along the center line of the main flow path are shown in Fig. 7. The spectra appear to be a combination of those on the right and left sides of the main flow path (Figs 5 & 6). For 80% void fraction, at both 5 m/s and 10 m/s pitch flow velocity, the spectra are very similar to those of the left side of the main flow path (Fig. 6). On the other hand the magnitudes of power spectral density of the higher frequency peak (11 Hz for 5 m/s pitch flow velocity, and 16 Hz for 10 m/s pitch flow velocity) are getting smaller. This means that the effect of the flow oscillation in the wake between the upstream and downstream cylinders becomes gradually weaker from the left to the center of the main flow path.

Further tests revealed the same trend, which is that the magnitudes of power spectral density of the higher frequency peak are getting smaller, and that the lower frequency peaks are getting more prominent relative to the higher frequency peak when the probes are traversed from the left to the right direction.

Some interesting trends may be observed by comparing the spectra of Probes L60° and U60°. For Probe L60°, the power spectral density is getting smaller (Figs 5(a), 6(a) and 7(a) or Figs 5(e), 6(e) and 7(e)), when the probe is moved from left to right. On the other hand, for Probe U-60°, the power spectral density is getting larger (Figs 5(c), 6(c) and 7(c) or Figs 5(g), 6(g) and 7(g)), when the probe is moved from left to right. Except for the near 11 and 16 Hz peaks (corresponding to a pitch flow velocity of 5 and 10 m/s respectively), the power spectral density of the void fraction fluctuations at positions L60°-L and U60°-R are somewhat similar as expected because of symmetry in the flow path. As shown in Fig. 3 the main flow path is essentially a series of 60° elbows. Positions L60°-L and U60°-R are similarly located on the elbows. More precisely, L60°-L and U60°-R are the extrados, L60°-R and U60°-L are the intrados at the exits of the two successive 60° elbows [11].

The 11 and 16 Hz peaks, on the other hand are due to the oscillating nature of the flow at the center of the test section between upstream and downstream cylinders. These oscillations are largely prevented by the presence of the wall between half-cylinders at the side of the test section.

Typical power spectra of local void fraction fluctuations at positions $U90^\circ-L_0$ and $U90^\circ-L_1$ are shown in Fig. 8. For 80% void fraction, at both 5 m/s and 10 m/s pitch flow velocity, the spectra at position L_0 (Figs 8(a) and 8(c)) are very similar to those of the center line of the main flow path (Figs 7(d) and 7(h)), except that the magnitudes of power spectral density are higher at L_0 . The spectra at position L_1 (Figs 8(b) and 8(d)) are very similar to those of the left side of the main flow path (Figs 6(d) and 6(h)) in both magnitude and frequency. This may be explained by the following observation.

Fig. 9(a) gives a simplified schematic representation of the flow structure inside a rotated triangular tube bundle. The flow is exclusively inside the flow path (FP) shown on Fig. 9(a). In between adjacent tubes of the same column (Tubes 1 and 2), the flow velocity is much less than in the flow paths and is taken to be near zero. This zone is called the stagnation zone or recirculation zone (SZ). In two-phase continuous flow, the mixture inside the flow paths appears to be very fine and homogenous. On the other hand, in the stagnation zone (SZ), the two-phase mixture is coarse and non-homogeneous, and transverse oscillations in the wake of the cylinders exist. Fig. 9(b) shows a black and white picture of the structure of the two-phase flow inside the rotated triangular array for high void fraction (95%) and flow velocity (12 m/s). Except for the tubes themselves, light tones indicate high void fraction mixtures and dark tones indicate very low void fraction two-phase mixtures. From Fig. 9(b), it can be seen that there is a large volume of very low void fraction mixture inside the stagnation zone and that a small portion of the space is occupied by a high void fraction mixtures. Similar phenomena were observed visually for 80% void fraction at 5 and 10 m/s pitch flow velocity.

The above investigation showed that the quasi-periodic drag and lift forces are generated by different mechanisms. The quasi-periodic drag forces appear related to the momentum flux fluctuations in the main flow path between the cylinders. The quasi-periodic lift forces, on the other hand, are mostly correlated to the oscillation in the wake of the cylinders.

3.3 Correlation between void fraction fluctuations and dynamic lift and drag forces

Further evidence of the correlation between void fraction fluctuations and the dynamic lift and drag forces is given in Fig. 10, which show the coherence between the void fraction fluctuations at $L60^\circ-C$ and $U90^\circ-L$ and the dynamic lift and drag forces for 80% void fraction at 5 m/s and 10 m/s pitch flow velocity. Figs 10(a) and 10(b) show that the coherence between void fraction fluctuations at $L60^\circ-C$ and drag forces is relatively high in the frequency range 0-20 Hz. Figs 10(c) and 10(d) reveal that the coherence between void fraction fluctuation at $U90^\circ-L$ and lift forces is relatively high up to 20 Hz for 5 m/s pitch flow velocity and 25 Hz for 10 m/s pitch flow velocity. It seems that the coherence between void fraction fluctuations at $U90^\circ-L$ and lift forces is somewhat better than the coherence between void fraction fluctuations at $L60^\circ-C$ and drag forces. More results on the coherence between void fraction fluctuations and the dynamic lift and drag forces at the quasi-periodic frequency for 80% void fraction at 5 m/s and 10 m/s pitch flow velocity may be found in Tables 1 and 2. On the whole, the coherence is higher at 10 m/s than at 5 m/s pitch flow velocity. For the coherence between void fraction fluctuations and the dynamic lift forces, this is probably because the wake oscillation phenomenon is steady and better defined at the higher pitch flow velocity as observed visually. For the same reason, the spectra of the void fraction fluctuation are narrower at the higher pitch flow velocity (Fig. 6).

3.4 Result from the wider test section

One may have the opinion that the present observations are possibly an artifact of this particular experimental set-up and would not be observed in another configuration of the same array geometry and flow conditions. This particular tube array may be too narrow to permit diffusion of the flow laterally across the wake area between upstream and downstream cylinders, a phenomenon perhaps even more important in two-phase flows because of void differences between the main flow path and the wake area between upstream and downstream cylinders. To answer these questions we have recently done some tests with a similar but wider test section including three columns of cylinders instead of one (Fig. 1(c)). Six cylinders located in the positions (L3, L4, R3, R4, C3, C5) were instrumented via strain gages. Similar results were found.

Typical lift and drag force spectra in the wider test section are shown in Figs 11 and 12. The lift force spectra reveal narrow band or quasi-periodic forces similar to those in the narrow test section. For the case of 80% void fraction, at both 5 and 10 m/s pitch flow velocity, the lift periodic frequency in the center column is a little higher than that in the narrow test section, although the amplitudes are quite similar. On the other hand, the lift periodic frequencies in adjacent columns (left and right columns) are similar to those in the narrow test section, although the amplitudes are a little less (Figs 11(a), (b), (c) and 12(a), (b), (c)). The difference in frequency may be related to the fact that the flow paths on each side of the columns are not identical. The two adjacent columns have a solid flow boundary on one side and an open flow boundary on the other side. On the other hand the center column has two open flow boundaries. Interestingly, some components of the drag force frequency may be found in the lift force spectra. Further tests revealed that the presence of drag force components in the lift force spectra is much less pronounced when the pitch flow velocity is less than 5 m/s.

Periodicity was also observed in the drag direction as shown in Figs 11(d), (e), (f) and Figs 12(e), (f), (g). For the case of 80% void fraction, at 5 m/s pitch flow velocity, the drag periodic frequency in both adjacent columns (L3, L4 and R3, R4) and for the centre column (C3, C5) is coincident with that in the narrow test section, although the amplitude seems smaller than that in the narrow test section (Figs 11(d), (e), and (f)). For the case of 80% void fraction, at 10 m/s pitch flow velocity, the drag force spectra show that two nearly similar peaks exist (Figs 12(e), (f), (g)). Both frequency and amplitude of the first peak are quite different than those of the drag force peak in the narrow test section (Fig. 12(h)). The second peak may be expected from periodic lift components. It also reveals that the interaction between the two periodic force mechanisms are more pronounced in the wider test section when the pitch flow velocity is greater than 5 m/s.

In summary quasi-periodic lift and drag forces essentially similar to those in the narrow test section also exist in the wider test section.

4. CONCLUSION

The results of two-phase flow dynamic characteristics and force measurements indicate that quasi-periodic drag and lift forces are generated by different mechanisms that have not been observed so far. The quasi-periodic drag forces appear related to the momentum flux fluctuations in the main flow path between the cylinders. These momentum flux fluctuations are caused by the void fraction fluctuations in the main flow path between the cylinders. The quasi-periodic lift forces, on the other hand, are mostly correlated to the oscillation in the wake of the cylinders. The quasi-periodic lift forces are related to local void fraction measurements in the unsteady wake

area between upstream and downstream cylinders. The quasi-periodic drag forces correlate well with similar measurements in the main flow stream between cylinders.

5. ACKNOWLEDGMENTS

The authors are grateful to Dragos Pamfil and Christine Monnette for the test section design and the development of the fiber-optic probes. Thanks are also due to Thierry Lafrance, Bénédicte Besner and Nour Aimène for their help throughout the project.

6. NOMENCLATURE

f : Frequency (Hz)

P, D : Pitch and tube diameter (m)

U_p : Pitch flow velocity (m/s)

$\alpha(t)$: Instantaneous local void fraction

7. REFERENCES

[1] Blevins, R. D., 1991, "Flow-induced vibration", New York: Van Nostrand Reinhold, 2nd edition.

[2] Axisa, F., Antunes, J., and Villard, B., 1990, "Random excitation of heat exchanger tubes by cross-flows", *Journal of Fluid and Structures*, 4, pp. 321-341.

[3] De Langre, E., and Villard, B., 1998, "An upper bound on random buffeting forces caused by two-phase flows across tubes", *Journal of Fluids Structures*, 12, pp. 1005–1023.

[4] Feenstra, P.A., Weaver, D.S., and Nakamura, T., 2003, "Vortex shedding and Fluid-elastic instability in a normal square tube array excited by two-phase Cross-flow", *Journal of Fluids and Structures*, 17, pp. 793–811.

[5] Nakamura, T., Fujita, K., Kowanishi, N., Yamaguchi, N., and Tsuge, A., 1995, "Study on the Vibration Characteristics of a Tube Array Caused by Two-Phase Flow, Part 1: Random Vibration", *Journal of Fluids and Structures*, 9, pp. 519–538.

[6] Pettigrew, M.J., and Taylor, C.E., 1994, "Two-phase flow-induced vibration: an overview", *ASME Journal of Pressure Vessel Technology*, 116, pp. 233-253.

[7] Pettigrew, M.J., Taylor, C.E. and Kim, B.S., 2001, "The effects of bundle geometry on heat exchanger tube vibration in two-phase cross-flow", *ASME Journal of Pressure Vessel Technology*, 123, pp. 414–420.

[8] Pettigrew, M.J., Taylor, C.E., Janzen, V. P., and Whan, T., 2002, "Vibration behavior of rotated triangular tube bundles in two-phase cross-flow", *ASME Journal of Pressure Vessel Technology*, 124, pp. 144–153.

[9] Taylor, C.E., Currie, I.G., Pettigrew, M.J. and Kim, B.S., 1989. "Vibration of tube bundles in two-phase cross-flow". Part 3: Turbulent induced excitation. *ASME Journal of Pressure Vessel Technology*, 111, pp. 488–500.

[10] Taylor, C. E., Pettigrew, M. J., and Currie, I. G., 1996, "Random excitation forces in tube bundles subjected to two-phase cross-flow", ASME Journal of Pressure Vessel Technology, 118, pp. 265-277.

[11] Pettigrew, M.J., Zhang, C, Mureithi, N.W, and Pamfil, D., 2005, "Detailed flow and force measurements in a rotated triangular tube bundle subjected to two-phase cross-flow", Journal of Fluids and Structures, 20, pp. 567-575.

[12] Zhang, C., Pettigrew, M.J., and Mureithi, N.W., 2006, "Vibration excitation force measurements in a rotated triangular tube bundle subjected to two-phase cross-flow", accepted for publication in ASME Journal of Pressure Vessel Technology.

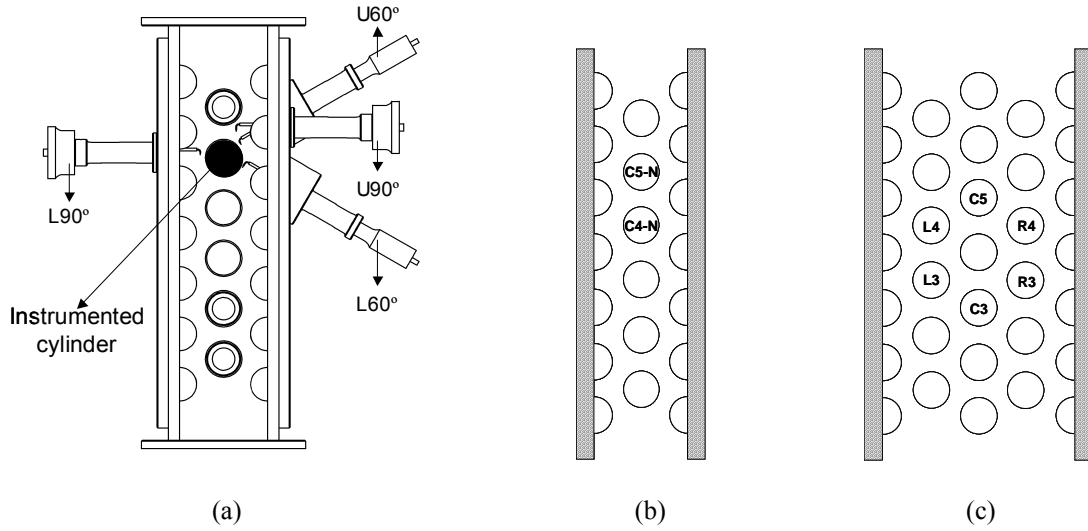


Figure 1: Test sections

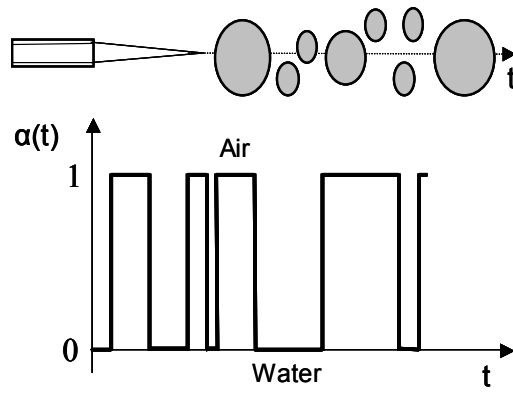


Figure 2: Idealized two-phase flow signal from fiber-optic probes

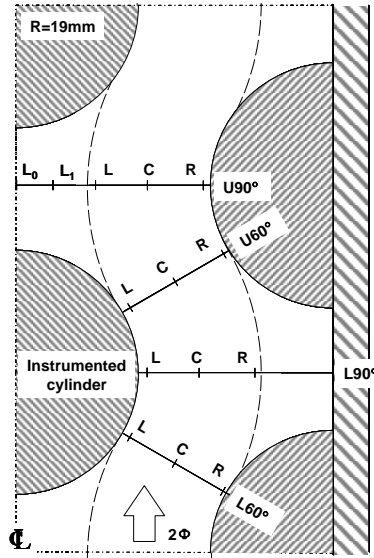


Figure 3: Probe positions for flow measurements

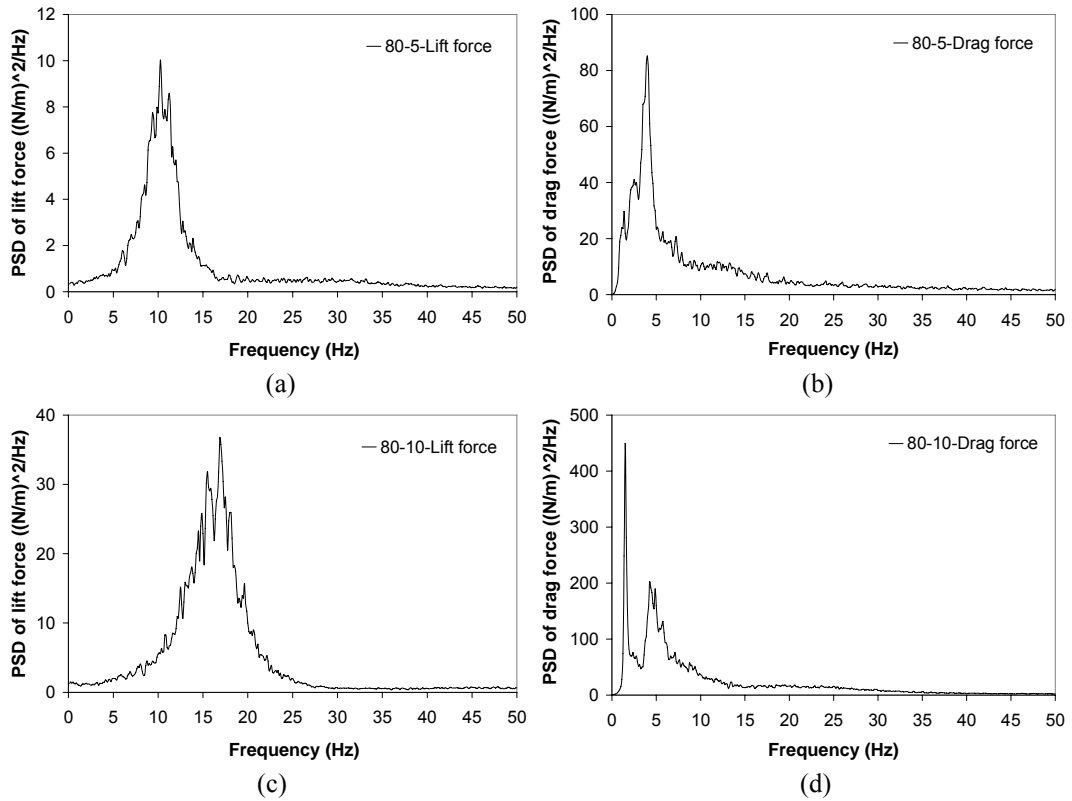


Figure 4: Typical dynamic force spectra for 80% void fraction at 5 and 10 m/s pitch flow velocity respectively; (a), (c) Lift force spectra, (b), (d) Drag force spectra

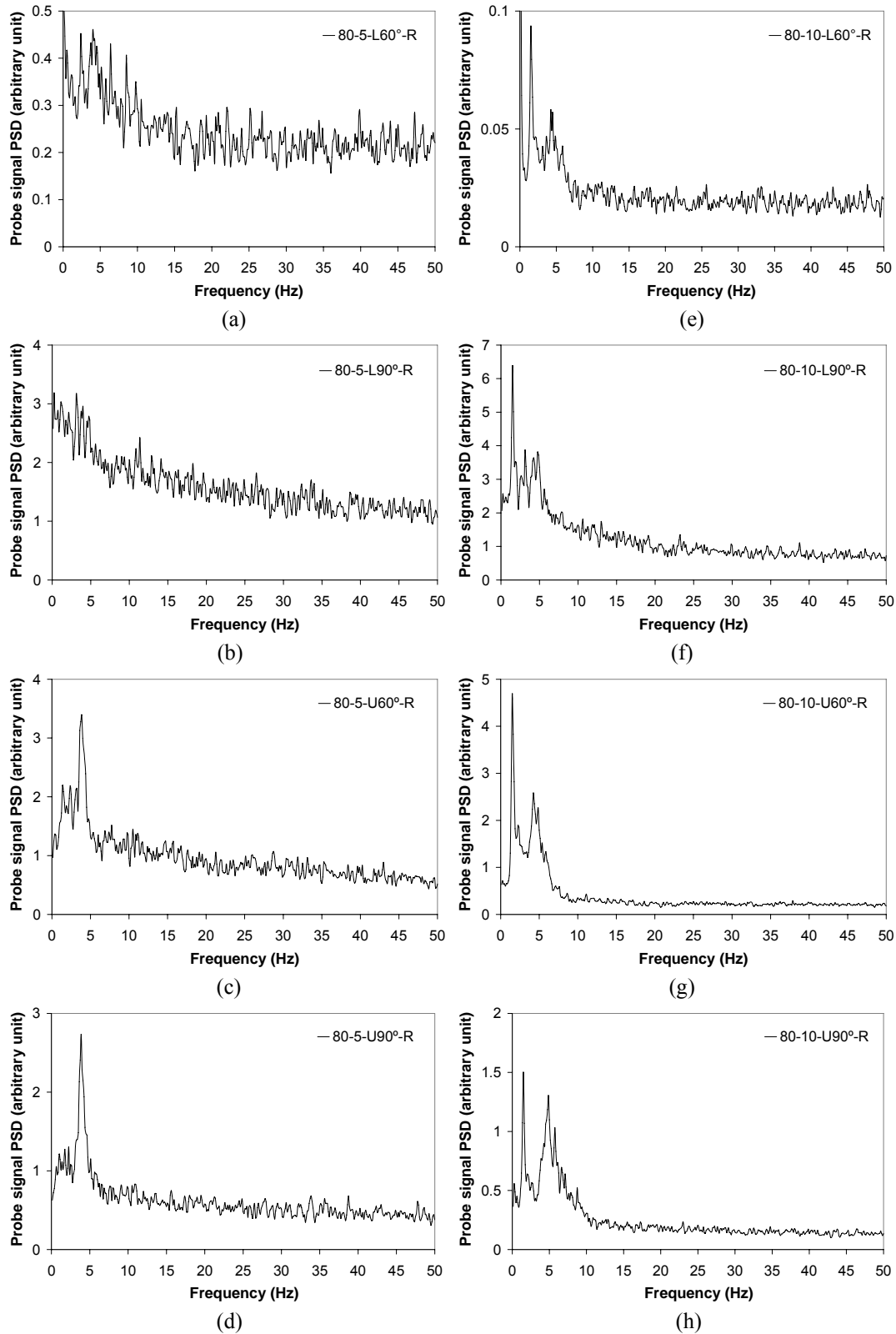


Figure 5: Power spectra of the local void fraction fluctuation at four different positions on the right side of the main flow path for 80% void fraction; pitch flow velocity 5 m/s, (a), (b), (c) and (d) and 10 m/s, (e), (f), (g) and (h); probe position, (a), (e) L60°, (b), (f) L90°, (c), (g) U60° and (d), (h) U90°

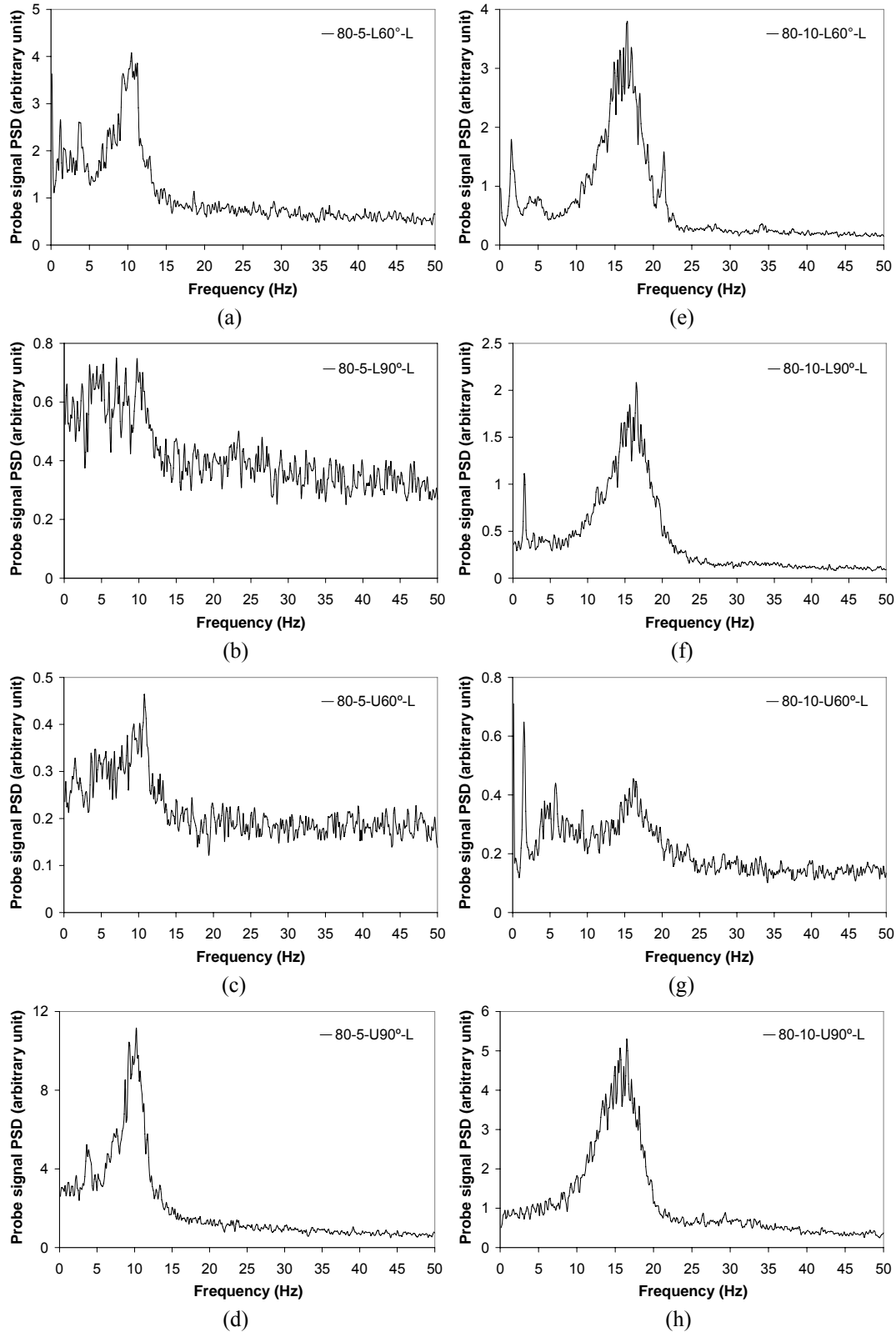


Figure 6: Power spectra of the local void fraction fluctuation at four different positions on the left side of the main flow path for 80% void fraction; pitch flow velocity 5 m/s, (a), (b), (c) and (d) and 10 m/s, (e), (f), (g) and (h); probe position, (a), (e) L60°, (b), (f) L90°, (c), (g) U60° and (d), (h) U90°

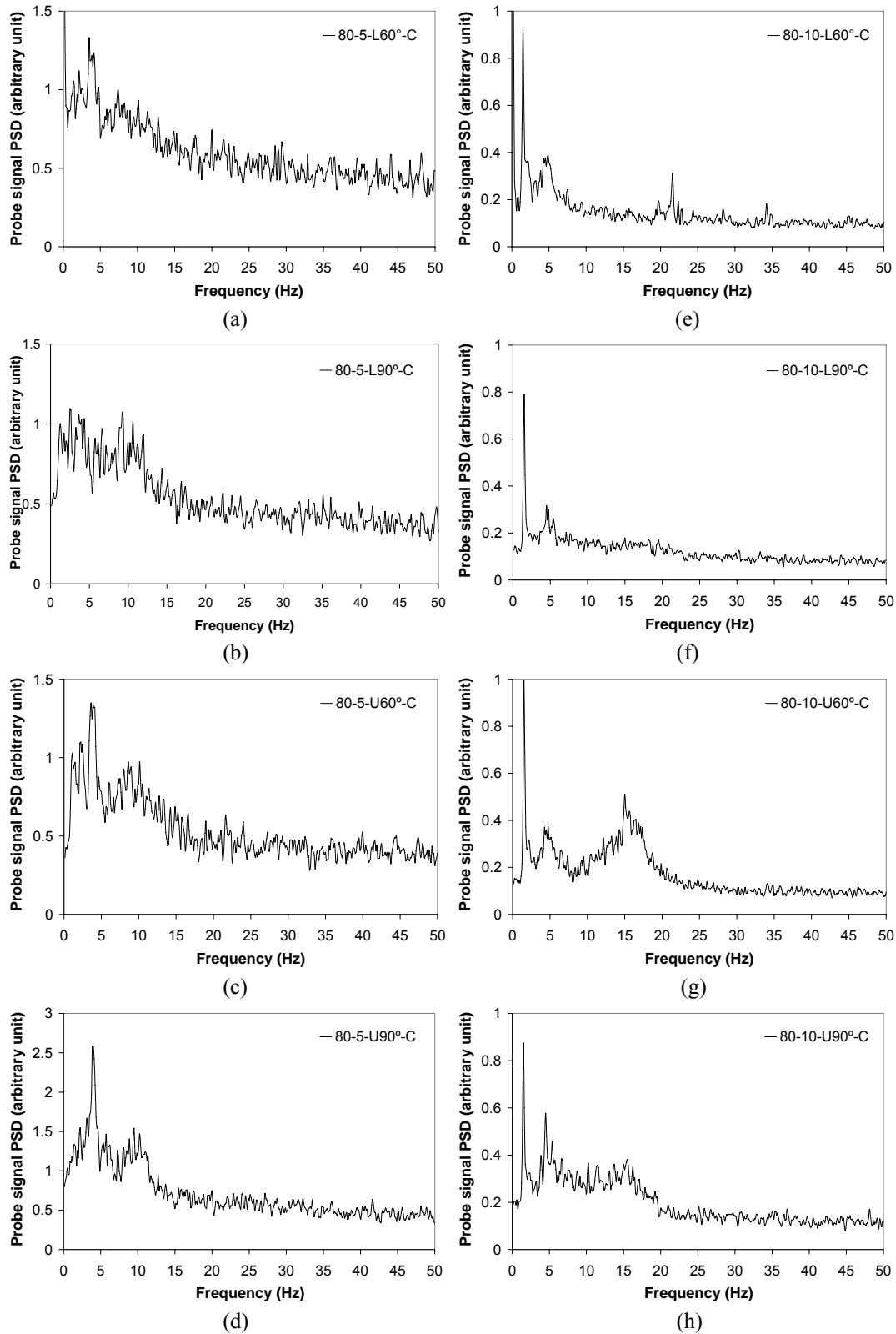


Figure 7: Power spectra of the local void fraction fluctuation at four different positions along the center line of the main flow path for 80% void fraction; pitch flow velocity 5 m/s, (a), (b), (c) and (d) and 10 m/s, (e), (f), (g) and (h); probe position, (a), (e) L60°, (b), (f) L90°, (c), (g) U60°, and (d), (h) U90°

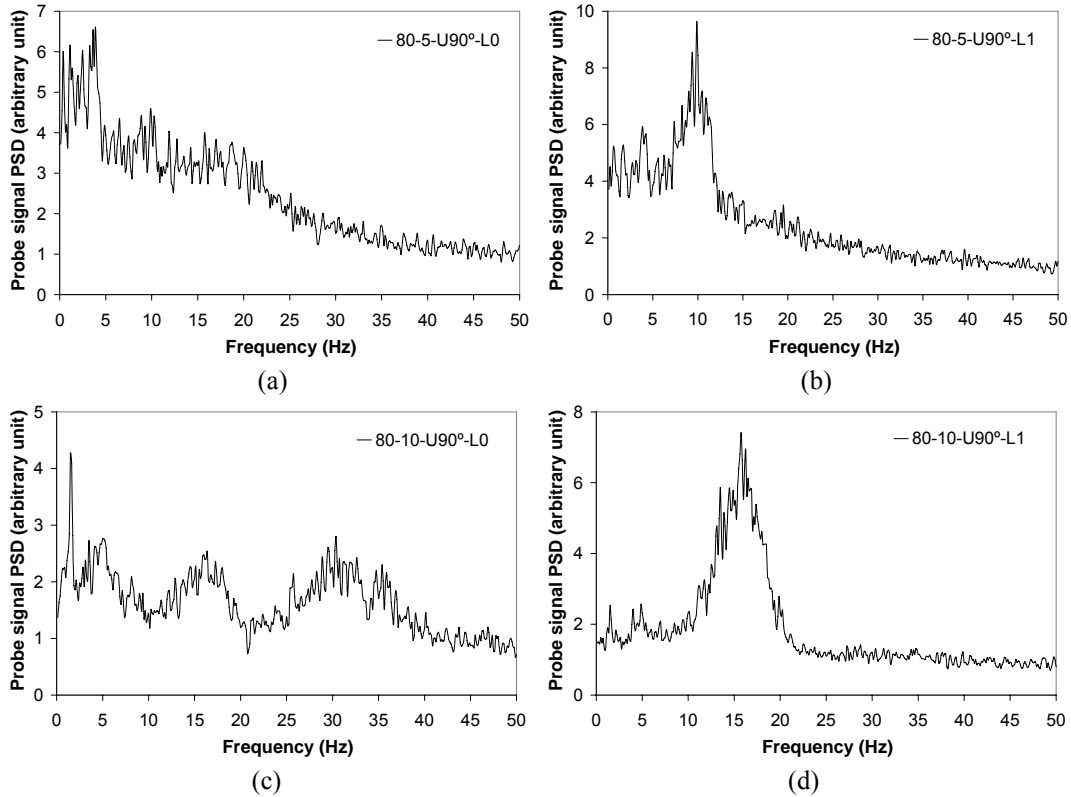


Figure 8: Power spectra of the local void fraction fluctuation at points L_0 and L_1 of U_{90° position; (a), (b) for 80% void fraction at 5 m/s pitch flow velocity, and (c), (d) for 80% void fraction at 10 m/s pitch flow velocity, respectively

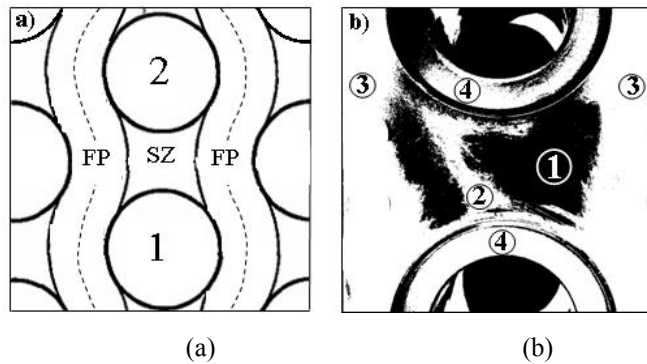


Figure 9: Two-phase flow structure in a rotated triangular tube bundle: a) simplified figure (FP: flow path, SZ: Stagnation zone), b) flow picture (1: low void fraction mixture belonging to the stagnation zone, 2: oscillating high void fraction mixture in stagnation zone, 3: flow path, 4: rigid tubes)

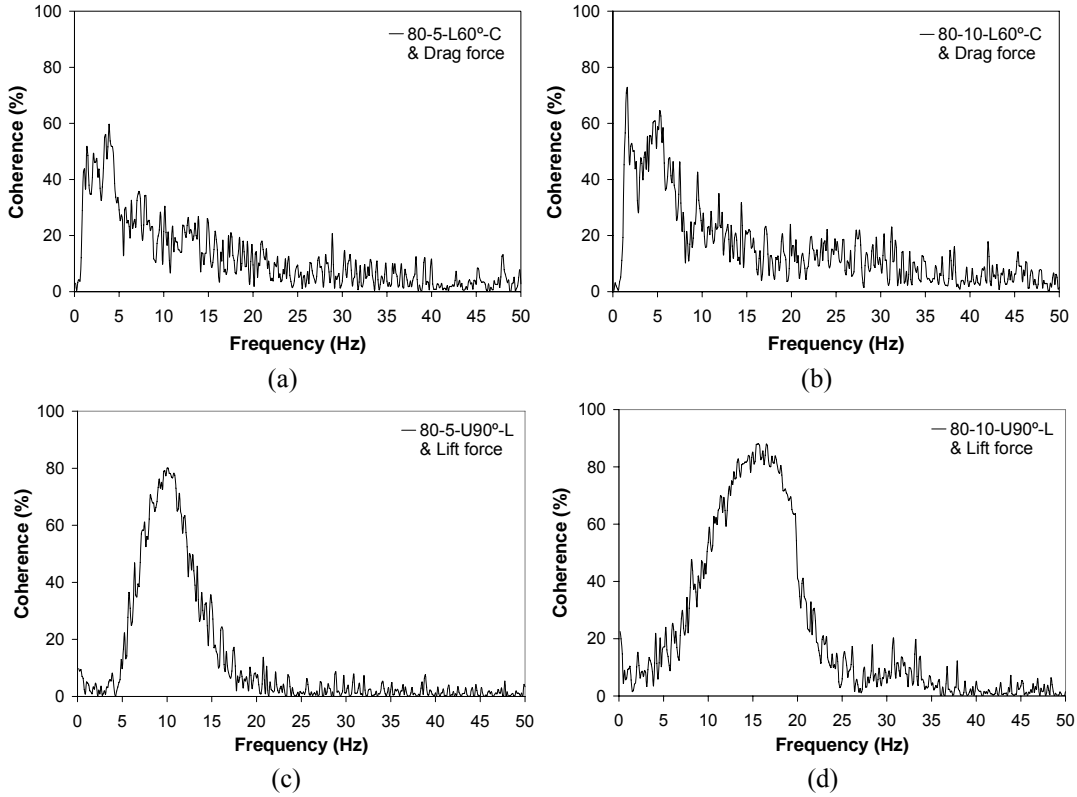


Figure 10: Coherences between the local void fraction fluctuation and the dynamic lift and drag forces for 80% void fraction; (a), (b) void fraction fluctuation at L60°-C and drag force, and (c), (d) void fraction fluctuation at U90°-L and lift force, at 5 m/s and 10 m/s pitch flow velocity, respectively

Probe positions Coherence (%)	In the bundle Within the main flow path	L60°	L90°	U60°	U90°
		With drag force	Center line	59.7	47.4
	Right side	37.2	11.1	65.6	76.2
	Left side	57.4	33.8	88.9	50.8
With lift force	Left side	71.6	21	54.6	80

Table 1: Coherence between void fraction fluctuations and the dynamic lift and drag forces at the quasi-periodic frequency for 80% void fraction at 5 m/s pitch flow velocity

Probe positions Coherence (%)	In the bundle Within the main flow path	L60°	L90°	U60°	U90°
		With drag force	Center line	64.5	57.4
	Right side	41.3	43.4	80.7	75.1
	Left side	52.6	25.9	49.6	26
With lift force	Left side	91.1	92.6	59.3	87.5

Table 2: Coherence between void fraction fluctuations and the dynamic lift and drag forces at the quasi-periodic frequency for 80% void fraction at 10 m/s pitch flow velocity

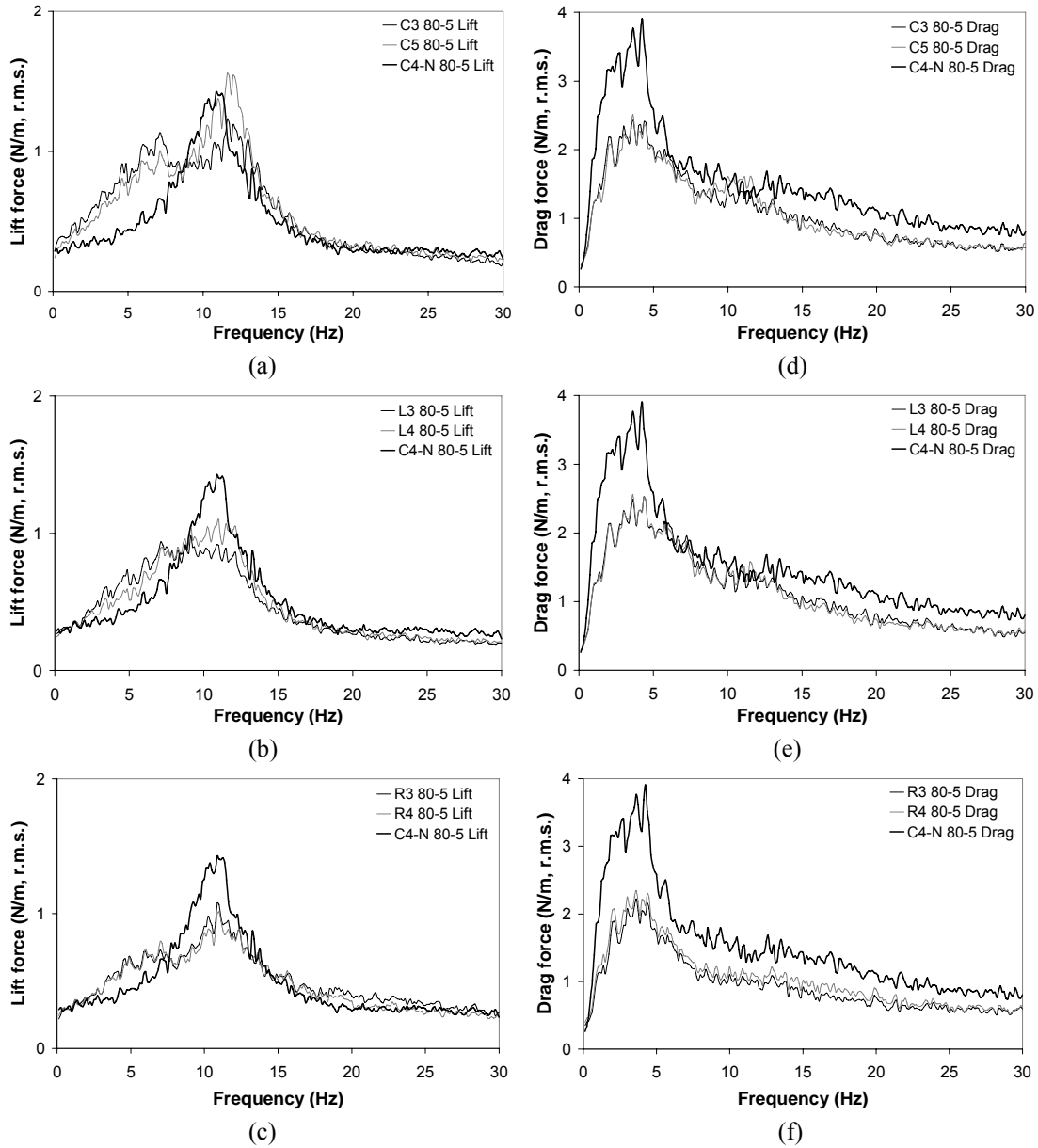


Figure 11: Comparison of the lift and drag forces in between the wider test section and the narrow test section for 80% void fraction at 5 m/s pitch flow velocity; (a), (b) and (c) for lift forces, and (d), (e) and (f) for drag forces, respectively

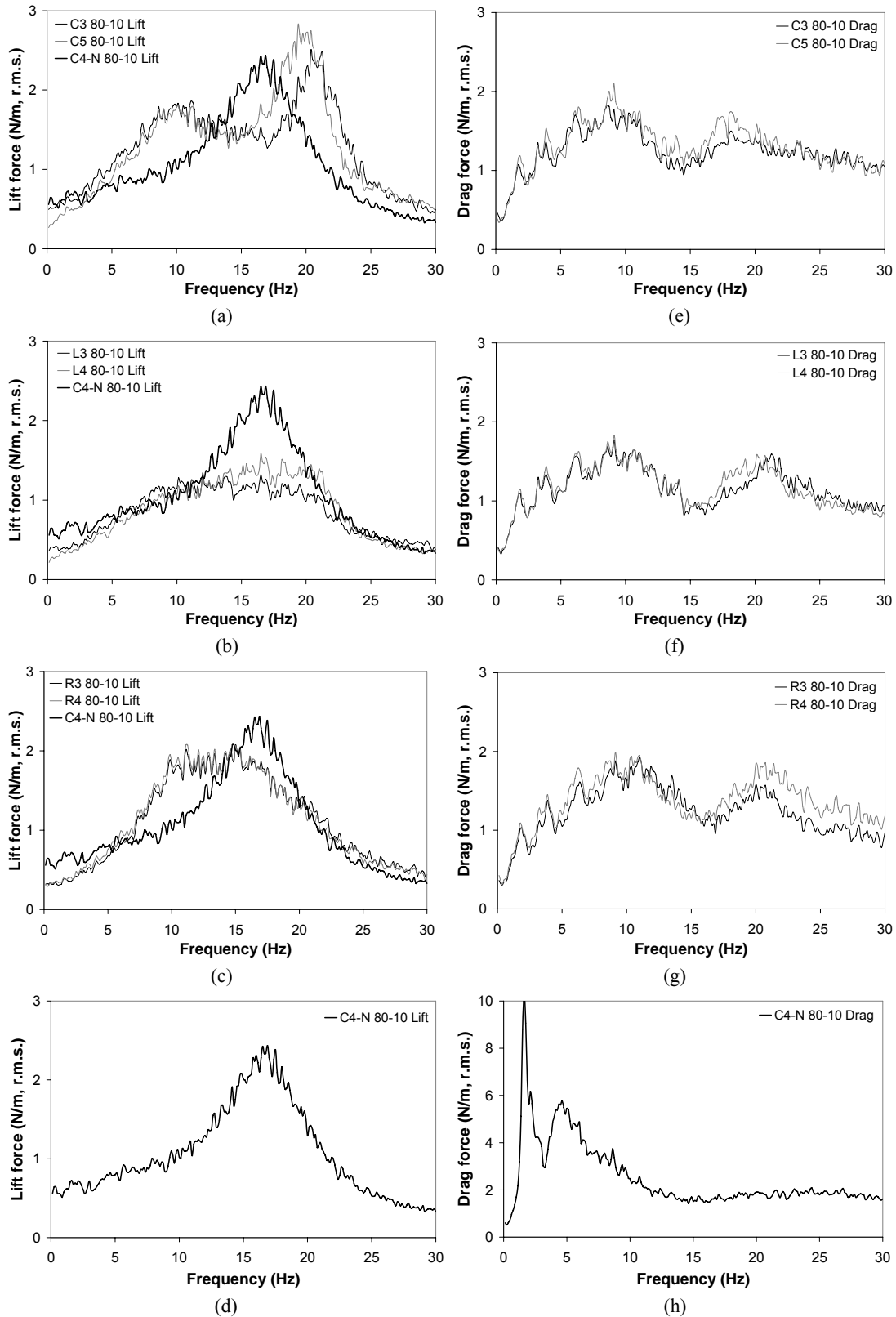


Figure 12: Comparison of the lift and drag forces in between the wider test section and the narrow test section for 80% void fraction at 10 m/s pitch flow velocity; (a), (b), (c) and (d) for lift forces, and (e), (f), (g) and (h) for drag forces, respectively